Selection of steady states in the two-dimensional symmetric model of dendritic growth

Daniel I. Meiron
Applied Mathematics Option, Firestone Laboratory, California Institute of Technology, Pasadena, California 91125
(Received 16 September 1985)

Selection of steady needle crystals in the full nonlocal symmetric model of dendritic growth is considered. The diffusion equation and associated kinematic and thermodynamic boundary conditions are recast into a nonlinear integral equation which is solved numerically. For the range of Péclet numbers and capillarity lengths considered it is found that a smooth solution exists only if anisotropy is included in the capillarity term of the Gibbs-Thomson condition. The behavior of the selected velocity and tip radius as a function of undercooling is also examined.

I. INTRODUCTION

It is well known that when a solid freezes into a supercooled melt the solid-liquid interface can become dendritic. The understanding of this process is of great importance to metallurgists since the properties of the solidified material will depend crucially on the details of the solidification process. The phenomenon of dendritic growth is also of great physical interest since it is a nonequilibrium dissipative process which spontaneously generates interfacial patterns.

The dynamics of dendritic growth can be viewed as a nonlinear Stefan problem in which the temperature and solute satisfy diffusion equations in both the solid and liquid phases and the motion of the interface is determined by the conservation of heat and the thermodynamic effects at the solid-liquid boundary. If one simply assumes that the interface is in local equilibrium, so that the interfacial temperature is just the melting temperature, then an exact solution due to Ivantsov[1] is known. In the Ivantsov theory the interface is simply a uniformly translating isothermal parabola. There are, however, two principal difficulties with the Ivantsov theory. The first is that for a given undercooling the Ivantsov solution is degenerate since it predicts only the product of the radius of curvature at the tip of the dendrite and the velocity. Experimentally it is known that several properties of dendritic growth do not depend on the time history of the interface. In particular, the radius of curvature and velocity of an advancing dendrite tip are reproducible functions of the thermal undercooling and the properties of the material but do not seem to depend on the way in which the dendrite was generated. In other words, for a given undercooling a unique velocity and radius of curvature are selected.[2] The degeneracy in the Ivantsov theory corresponds to a scale invariance and it is necessary to add some additional physical information to set the scale and allow for the solution of both the velocity and radius of curvature. The second theoretical difficulty is that the Ivantsov solution is unstable with the growth rate increasing as the disturbance wavelength decreases. This is again related to the degeneracy of the solution.

It has been suggested that since the capillarity and molecular attachment effects provide an additional scale, their inclusion into the thermodynamic boundary condition should facilitate a prediction of the velocity-undercooling relationship. The addition of capillarity in the problem, however, makes it analytically intractable. There have been several attempts to include capillarity in an approximate manner. Notable among these are the hypotheses of marginal stability and maximum velocity.

The marginal-stability hypothesis[3] uses the Ivantsov needle as an approximate basic state and examines its stability in the presence of capillarity. The inclusion of capillarity introduces a stability length such that disturbances with a wavelength shorter than the stability length are damped. This has the effect of rendering some of the Ivantsov needles completely stable. The hypothesis states that the tip velocity is that which is due to the Ivantsov needle, which is just stabilized by capillarity. For further details the reader is referred to the comprehensive review of Langer.[4]

The maximum velocity hypothesis of Nash and Glicksman is based on a numerical solution of the full nonlinear boundary value problem in three dimensions. Nash and Glicksman[5] derived a nonlinear integral equation for the shape of the boundary and solved it by Newton's method. In their calculations the addition of capillarity yields a state of maximum velocity for a given undercooling and it is this state that is selected by the dynamics.

Both of these approaches to the problem of velocity selection are predicated on the notion that the smoothness of the Ivantsov solution is not affected by the inclusion of the capillarity terms and that for sufficiently small values of the characteristic capillarity length the Ivantsov solution is modified but remains degenerate.[6]

The intractability of the full problem has led to the introduction of local models of dendritic growth. These are evolutionary equations for the interfacial curvature constructed so as to model some aspects of the full nonlocal problem. The obvious advantage of this approach is that it avoids the complications of solving the diffusion equation while at the same time retains some of the phenomenology. Two examples of this approach are the geometrical model of Brower *et al.*[7] and the boundary layer model of Ben-Jacob *et al.*[8] Both models possess equivalents of the Ivantsov needle solution and are sufficiently tractable so that it can be shown that the continu-

um of the Ivantsov solutions does not survive in the presence of capillarity.[9] Most of the solutions become inadmissible as they develop singularities at the needle tip. The velocities and tip radii of those solutions which remain smooth now form a discrete set. In the numerical simulations of Kessler *et al.*[9] the selected steady state is the member of the discrete set which has the largest tip velocity. This new selection criterion has been dubbed microscopic solvability since it is now the solvability condition that the solution remain smooth at the tip which fixes the velocity.

Motivated by these findings we have investigated the existence of steady states in the presence of capillarity for the two-dimensional full nonlocal model of dendritic growth. We have followed Nash and Glicksman in reformulating this problem as a nonlocal integral equation but we have not imposed any conditions on the smoothness of the solution at the tip. We solve this equation numerically using Newton's method. Our methodology is described in Sec. II. We find that nontrivial needle-crystal solutions exist only in the presence of capillarity which accounts for crystalline anisotropy. In our calculations we have imposed a fourfold anisotropy in the capillarity term. Our numerical calculations are neither exhaustive nor rigorous but they nevertheless suggest that anisotropy plays a crucial role in the selection of dendrite-tip velocities and radii. Detailed results of our calculations are presented in Sec. III and some conclusions in Sec. IV.

II. MATHEMATICAL AND NUMERICAL FORMULATION

We consider the motion of a solid-liquid interface $z(x)$, which occurs due to solidification into an undercooled melt. The heat budgets in both the solid and liquid phases are assumed to be controlled by diffusion so that the temperature fields T_S, T_L in the solid and liquid, respectively, obey

$$D_{T_S}\nabla^2 T_S = \frac{\partial T_S}{\partial t} , \tag{2.1}$$

$$D_{T_L}\nabla^2 T_L = \frac{\partial T_L}{\partial t} , \tag{2.2}$$

where D_{T_S} and D_{T_L} are the thermal diffusion constants. The motion of the interface is determined by the rate at which latent heat is diffused into the bulk phases. The normal velocity $\mathbf{v}\cdot\hat{\mathbf{n}}$ of the interface is determined from the heat conservation condition

$$L\,\mathbf{v}\cdot\hat{\mathbf{n}} = (D_{T_S}c_{pS}\nabla T_S - D_{T_L}c_{pL}\nabla T_L)\cdot\hat{\mathbf{n}} . \tag{2.3}$$

Here L is the latent heat per unit volume and c_{pS}, c_{pL} are the specific heats for the two phases. It is understood that the gradients are evaluated at the interface. If we assume that $c_{pS}=c_{pL}=c_p$ and measure temperature in units of c_p/L, Eqs. (2.1), (2.2), and (2.3) become

$$D_{T_S}\nabla^2 T_S = \frac{\partial T_S}{\partial t} , \tag{2.4}$$

$$D_{T_L}\nabla^2 T_L = \frac{\partial T_L}{\partial t} , \tag{2.5}$$

$$\mathbf{v}\cdot\hat{\mathbf{n}} = (D_{T_S}\nabla T_S - D_{T_L}\nabla T_L)\cdot\hat{\mathbf{n}} . \tag{2.6}$$

In order to uniquely fix the shape of the interface we must also impose a thermodynamic boundary condition. The thermodynamic condition used here is a form of the Gibbs-Thomson relation

$$T\,|_{\text{interface}} = T_M - \frac{\gamma}{L} f(\theta)\kappa , \tag{2.7}$$

where T_M is the melting temperature, κ is the interfacial curvature defined to be positive if the center of curvature lies on the solid side of the interface, γ/L is the capillarity length, and θ represents the angle between the outward-pointing normal $\hat{\mathbf{n}}$ and the vertical axis. The function $f(\theta)$, which in general depends on the geometric parameters of the interface, represents a measure of the anisotropy in the Gibbs-Thomson term. Its explicit form will be indicated later. As pointed out by Langer the simple condition (2.7) represents an assumption of local equilibrium and ignores potentially important effects such as convection in the fluid. It is nevertheless an important first approximation in the study of solidification.

Our interest lies in computing the shapes of steadily advancing solidification fronts. In a frame of reference traveling with the front velocity $\mathbf{v}$ the diffusion equations become

$$\nabla^2 T_S + \frac{2}{l_S}\frac{\partial T_S}{\partial z} = 0 , \tag{2.8}$$

$$\nabla^2 T_L + \frac{2}{l_L}\frac{\partial T}{\partial z} = 0 , \tag{2.9}$$

where l_L and l_S are the diffusion lengths in the solid and liquid and are given by

$$l_S = \frac{2D_S}{v}, \quad l_L = \frac{2D_L}{v} . \tag{2.10}$$

We shall further assume that $l_S = l_L = l = 2D/v$. This corresponds to the symmetric model studied by Langer and Turski.[10] For most substances the diffusion constants are not equal in the liquid and solid phases but it should be noted that succinonitrile, a widely used material in the experimental studies of dendritic growth, does possess nearly symmetric diffusion constants.[2] In this limit the temperature fields in the solid and liquid phases are governed by a single diffusion equation with the conservation condition

$$D\left[\frac{\partial T_S}{\partial n} - \frac{\partial T_L}{\partial n}\right] = \mathbf{v}\cdot\hat{\mathbf{n}} . \tag{2.11}$$

One interpretation of condition (2.11) is that the interface in the symmetric model acts as a source distribution and thus the solution in both the solid and liquid domains

may be expressed as an integral over the interface boundary of the form

$$T(\mathbf{r})=\int_{-\infty}^{\infty}\mu(s')G(\mathbf{r}\mid\mathbf{r}')ds' , \tag{2.12}$$

where $\mathbf{r}$ is an arbitrary vector, $\mathbf{r}'$ is a vector directed along the interface, ds' represents the element of surface area, μ is the source sheet strength, and $G(\mathbf{r}\mid\mathbf{r}')$ is the source Green's function for the elliptic equation

$$\nabla^2 T+\frac{2}{l}\frac{\partial T}{\partial_z}=0 . \tag{2.13}$$

The explicit form of the Green's function $G(\mathbf{r}\mid\mathbf{r}')$ is

$$G(\mathbf{r}\mid\mathbf{r}')=\frac{1}{2\pi}\exp\left[\frac{z(s')-z(s)}{l}\right]K_0\left[\frac{|\mathbf{r}(s)-\mathbf{r}(s')|}{l}\right] \tag{2.14}$$

in two dimensions, where K_0 is a modified Bessel function of zeroth order. Note that due to the behavior of the Green's function the temperature field is constrained to vanish in the liquid phase at large distances from the interface.

Using (2.12) we can rewrite the nonlinear boundary value problem posed by (2.7), (2.11), and (2.13) and the definition of the outward-pointing normal $\hat{\mathbf{n}}=[(-dz/ds),(dx/ds)]$ as a nonlinear integro-differential equation

$$\Delta-\frac{\gamma}{L}f(\theta)K=\frac{v}{2\pi D}\int_{-\infty}^{\infty}dx'\exp\left[\frac{z(x')-z(x)}{l}\right]K_0\left[\frac{\{(x-x')^2+[z(x)-z(x')]^2\}^{1/2}}{l}\right], \tag{2.15}$$

where Δ is the thermal undercooling. We now scale all lengths by the diffusion length $l=2D/v$ and find

$$\Delta-d_0 f\kappa=\frac{1}{\pi}\int_{-\infty}^{\infty}dx'\exp[z(x')-z(x)]K_0(\{(x-x')^2+[z(x)-z(x')]^2\}^{1/2}) . \tag{2.16}$$

Here $d_0=(\gamma/L)(v/2D)$ is the dimensionless capillarity length. It can be verified that in the absence of capillary effects ($d_0=0$) Eq. (2.16) reproduces the well-known Ivantsov solution in two dimensions. In our dimensionless variables this is

$$z(x)=\frac{-x^2}{2\mathcal{N}_{\text{Péclet}}} , \tag{2.17}$$

$$\Delta=\sqrt{\pi}(\mathcal{N}_{\text{Péclet}})^{1/2}\exp(\mathcal{N}_{\text{Péclet}})\operatorname{erfc}(\mathcal{N}_{\text{Péclet}})^{1/2} . \tag{2.18}$$

The Péclet number $\mathcal{N}_{\text{Péclet}}$ is given by $\mathcal{N}_{\text{Péclet}}=\rho_I/l$, where ρ_I is the radius curvature of the Ivantsov parabola.

While it is possible to verify that substituting the parabola (2.17) into the integrand yields a constant Δ, which obeys (2.18) through the use of identities among Bessel functions, this result can be seen directly from the derivation of Pelcé and Pomeau[11] who rewrite Eq. (2.16) using the free-space Green's function for the heat equation. In their formulation Eq. (2.16) becomes

$$\Delta-d_0^*\kappa=v\int_0^{\infty}\frac{d\tau}{(4\pi\tau)^{3/2}}\int_{-\infty}^{\infty}dx\int_{-\infty}^{\infty}dy\exp\left[-\frac{1}{4\tau}[(x-x_1)^2+(y-y_1)^2+(z-z_1+v\tau)^2]\right] . \tag{2.19}$$

After substituting the parabolic solution (2.17) into (2.19), a series of simple variable transformations are used to show that the integral in two dimensions is a function only of the Péclet number and not of the variable x.

In order to study the effects of anisotropy we have followed Karma *et al.*[9] and imposed a fourfold anisotropy in the curvature of the form

$$f(\theta)=1+\alpha(1-\cos 4\theta) , \tag{2.20}$$

where

$$\cos\theta=\frac{1}{\left[1+\left[\frac{dz}{dx}\right]^2\right]^{1/2}} . \tag{2.21}$$

It is also possible to treat anisotropic effects arising from the attachment kinetics of the crystal-growth process but we have not considered this type of anisotropy here.

The final form of the boundary integral equation to be studied is

$$\Delta+d_0[1+\alpha(8\cos^2\theta-8\cos^4\theta)]\frac{\dfrac{d^2z}{dx^2}}{\left[1+\left[\dfrac{dz}{dx}\right]^2\right]^{3/2}}=\frac{1}{\pi}\int_{-\infty}^{\infty}dx'\exp[z(x')-z(x)]K_0\{(x-x')^2+[z(x)-z(x')]^2\}^{1/2}\ . \tag{2.22}$$

Although Eq. (2.22) is a nonlinear nonlocal integral equation it does have the advantage of reducing a problem in two space dimensions to one in which the shape of the interface determines the solution everywhere. The principal numerical difficulties in solving (2.22) are the logarithmic singularity of the kernel as $x\to x'$ and that the problem is posed on the infinite interval $-\infty<x<\infty$. In addition, numerical experience in the solution of the Hele-Shaw fingering problem indicates that the curvature terms behave as singular perturbations so that high resolution will be required in order to obtain accurate solutions in the limit $d_0\ll 1$.[12]

The treatment of these difficulties follows closely the work of Nash and Glicksman.[5] We assume the solution is reflection symmetric about the z axis. This reduces the interval of integration to $0<x<\infty$ and Eq. (2.22) becomes

$$\Delta+d_0[1+\alpha(8\cos^2\theta-8\cos^4\theta)]\frac{\dfrac{d^2z}{dx^2}}{\left[1+\left[\dfrac{dz}{dx}\right]^2\right]^{3/2}}=\int_{-\infty}^{\infty}dx'\exp[z(x')-z(x)](K_0\{(x-x')^2+[z(x)-z(x')]^2\}^{1/2}+K_0\{(x+x')^2+[z(x)-z(x')]^2\}^{1/2})\ . \tag{2.23}$$

The integration domain is broken up into two parts: $0<x'<x_N$ and $x_N<x'<\infty$. The region $0<x'<x_N$ is further subdivided into smaller regions with the solution computed in detail in this region. From thermodynamic considerations it can be shown that as $x'\to\infty$, the solution $z(x)$ approaches the Ivantsov parabola. Thus for $x'>x_N$ we assume the solution is of the form

$$z(x)=A_{N+1}+B_{N+1}x+C_{N+1}x^2\ . \tag{2.24}$$

For x_N, large enough C_{N+1} will approach $-1/2\mathcal{N}_{\text{Péclet}}$, the Ivantsov solution. In general, the difference between the computed and expected value of C_{N+1} serves as a measure of the error in truncating the region of detailed computation. We select collocation points $0<x_1<x_2<\cdots<x_N$ and subdivide the region $0<x<x_N$ into elements where the ith element spans the region $x_{i-1}<x_i<x_{i+1}$; the solution $z(x)$ for the ith element is an interpolating parabola of the form

$$z_i(x)=A_i+B_ix+C_ix^2\ , \tag{2.25}$$

where the A_i, B_i, and C_i are chosen such that

$$z(x_{i-1})=z_{i-1},\quad z(x_i)=z_i,\quad z(x_{i+1})=z_{i+1}\ . \tag{2.26}$$

In other words the solution is spanned by local overlapping parabolas. Each point x_i is an end point of the $(i-1)$th and $(i+1)$th parabolas and lies in the interior of the ith parabola. We have not imposed any additional constraints such as continuity of the first derivative. The integral in (2.23) over the region $0<x<x_N$ becomes

$$F_1(j)=\sum_{i=0}^{N-1}\int_{x_i}^{x_{i+1}}dx'\exp[A_i+B_ix'+C_ix'^2-z(x_j)]\times(K_0\{(x_j-x')^2+[A_i+B_ix'+C_ix'^2-z(x_j)]^2\}^{1/2}+K_0\{(x_j+x')^2+[A_i+B_ix'+C_ix'^2-z(x_j)]^2\}^{1/2})=\sum_{i=0}^{N-1}(x_{i+1}-x_i)\int_0^1 G_{ij}(\beta)d\beta\ , \tag{2.27}$$

where

$$G_{ij}=\exp[a_i+b_i\beta+c_i\beta^2-z(x_j)][K_0(\{[x_j-\beta x_{i+1}-(1-\beta)x_i]^2+[a_i+b_i\beta+c_i\beta^2-z(x_j)]^2\}^2)+K_0(\{[x_j+\beta x_{i+1}+(1-\beta)x_i]^2+[a_i+b_i\beta+c_i\beta^2-z(x_j)]^2\}^{1/2})] \tag{2.28}$$

$$\begin{aligned}a_i&=A_i+B_ix_i+C_ix_i^2=z(x_i)\ ,\\ b_i&=(-2C_ix_i+B_i)(x_{i+1}-x_i)\ ,\\ c_i&=C_i(x_{i+1}-x_i)^2\ ,\end{aligned} \tag{2.29}$$

and

$$A_i=\frac{z_{i-1}x_ix_{i+1}}{(x_{i-1}-x_i)(x_{i-1}-x_{i+1})}+\frac{z_ix_{i-1}x_{i+1}}{(x_i-x_{i-1})(x_i-x_{i+1})}+\frac{z_{i+1}x_{i-1}x_i}{(x_{i+1}-x_{i-1})(x_{i+1}-x_i)},$$
$$B_i=-\frac{z_{i-1}(x_i+x_{i+1})}{(x_{i-1}-x_i)(x_{i-1}-x_{i+1})}-\frac{z_i(x_{i-1}+x_{i+1})}{(x_i-x_{i-1})(x_i-x_{i+1})}-\frac{z_{i+1}(x_{i-1}+x_i)}{(x_{i+1}-x_{i-1})(x_{i+1}-x_i)}, \tag{2.30}$$
$$C_i=\frac{z_{i-1}}{(x_{i-1}-x_i)(x_{i-1}-x_{i+1})}+\frac{z_i}{(x_i-x_{i-1})(x_i-x_{i+1})}+\frac{z_{i+1}}{(x_{i+1}-x_{i-1})(x_{i+1}-x_i)}.$$

In order to match to the parabola at $x=x_N$ (2.24) and to account properly for the end point at $x=0$ we apply the conditions

$$A_0=A_1,\ B_0=B_1,\ C_0=C_1,$$
$$A_{N+1}=A_N,\ B_{N+1}=B_N,\ C_{N+1}=C_N. \tag{2.31}$$

The integrands $G_{ij}(\beta)$ are well behaved for $i\neq j$ and $i\neq j-1$. The integrands for G_{ii} and $G_{i,i+1}$ have logarithmic singularities at $\beta=0$ and $\beta=1$, respectively. Although these singularities are integrable they must be isolated so that standard quadrature rules can be applied. We therefore rewrite these integrands as follows:

$$\int_0^1 G_{ii}(\beta)d\beta=\int_0^1 G_{ii}(\beta)-(1+p_{i0}\beta+q_{i0}\beta^2)\ln\beta\,d\beta+\frac{4q_{i0}+9p_{i0}+36}{36}, \tag{2.32}$$

$$\int_0^1 G_{i,i+1}(\beta)d\beta=\int_0^1 G_{i,i+1}(\beta)-[1+p_{i1}(\beta-1)+q_{i1}(\beta-1)^2]\ln|\beta-1|\,d\beta+\frac{4q_{i1}-9p_{i1}+36}{36}, \tag{2.33}$$

where

$$p_{i0}=b_i,$$
$$q_{i0}=c_i+\frac{3b_i^2}{4}+\tfrac{1}{4}(x_{i+1}-x_i)^2,$$
$$p_{i1}=b_i+2c_i,$$
$$q_{i1}=c_i+\tfrac{3}{4}(b_i+2c_i)^2+\tfrac{1}{4}(x_{i+1}-x_i)^2.$$

The leading-order behavior of the integrand is now $O(\beta^3\ln\beta)$ near the end points. This is sufficiently smooth so that standard Gauss-Legendre quadrature may be applied.

For the remainder of the region of integration $x_N<x<\infty$ the integral is given by

$$F_2(x_j)=\int_{x_N}^{\infty}dx'\exp[P_{N+1}(x')-z(x_j)]$$
$$\times[K_0(\{(x'-x)^2+[P_{N+1}(x')-z(x_j)]^2\}^{1/2})+K_0(\{(x'+x)^2+[P_{N+1}(x')-z(x_j)]^2\}^{1/2})]. \tag{2.34}$$

A logarithmic subtraction of the type described ab ve must be performed for the point $x_j=x_N$. The remainder of the integral is computed by mapping the infinite domain $x_N<x'<\infty$ onto $0<t<1$ by means of the algebraic transformation

$$x'=\frac{t}{1-t}+x_N.$$

The final form of equations (2.23) using the discretization described above is

$$\Delta+d_0[1+\alpha(8\cos^2\theta_j-8\cos^4\theta_j)]\frac{2C_j}{[1+(B_j+2x_jC_j)^2]^{3/2}}=F_1(j)+F_2(j),\quad j=1,2,\ldots,N \tag{2.35}$$

where

$$\cos\theta_j=\frac{1}{[1+(B_j+2x_jC_j)^2]^{1/2}}.$$

This equation is still invariant with respect to translations in z. Therefore, in order to render the solution unique we impose the boundary condition $A_0=0$. With this constraint and in the absence of capillarity ($d_0=0$) Eq. (2.35) has the discrete Ivantsov solution

$$z(x_i)=\frac{-x_i^2}{2\mathcal{N}_{\text{Péclet}}},$$
$$A_i=0,\ B_i=0,\ C_i=\frac{-1}{2\mathcal{N}_{\text{Péclet}}},\quad i=1,2,\ldots,N \tag{2.36}$$

$$\Delta=\sqrt{\pi}(\mathcal{N}_{\text{Péclet}})^{1/2}\exp\mathcal{N}_{\text{Péclet}}\operatorname{erfc}(\mathcal{N}_{\text{Péclet}})^{1/2} . \quad (2.37)$$

The equations (2.35) with the associated boundary conditions (2.31) now constitute a discrete nonlinear system for the interface nodes (x_i,z_i) and are solved by Newton's method. Numerical tests show that with a five-point Gaussian quadrature used to compute the elements G_{ij}, the Ivantsov solution (2.36) is reproduced to eight significant digits over the entire range $0<x<\infty$.

Note that in our formulation we do not constrain the slope at the tip to vanish. The diffusional kinetics which govern dendritic growth would favor solutions that are smooth at the origin. For this class of solutions the slope at the tip [from (2.31) the value of B_0] should vanish. Numerical work on the geometrical and boundary layer models have shown that the equivalent Ivantsov solution in both models does satisfy a smoothness criterion of this type but that solutions in the presence of capillarity in general do not; in these local models the condition that the solution remain smooth at the tip of the needle was satisfied only at selected values of the control parameter d_0. The existence of cusped needle crystals, while physically unlikely, would necessitate a modification of our equations near the tip. In addition, we have not examined the mathematical issues of existence associated with such weak solutions.

In our units the parameter d_0 is scaled by the diffusion length. Thus the smoothness criterion is also a velocity selection criterion since d_0 is linearly proportional to the velocity. This suggests a numerical strategy for locating smooth solutions. We begin by selecting a Péclet number and generating the corresponding Ivantsov parabola. As the parameter d_0 is increased the value of the slope at the tip (B_0) is monitored. In general, B_0 will not vanish, but if steady states in the presence of surface tension exist there will be a set of values d_0 at which $B_0=0$. Variants of this technique have been employed in the study of the geometrical and boundary layer models and by Vanden-Broeck[13] in his study of Hele-Shaw fingering.

Unless the slope at the tip vanishes it is, strictly speaking, undefined, but by symmetrizing about the z axis as we have done it can be given meaning as a one-sided limit. In effect we are computing solutions which are singular in that they have a cusp at the tip. As a result it is difficult to get estimates for the rate of convergence of the numerical method proposed above, and we have relied instead on repeated runs where the number of points N and the cutoff value x_N are varied.

III. RESULTS

In order to investigate the behavior of the slope at the tip for $d_0>0$, we calculated solutions for $\mathcal{N}_{\text{Péclet}}=0.01$, 0.1, 1, for values of d_0 in the range $0<d_0<2$ in the ab-

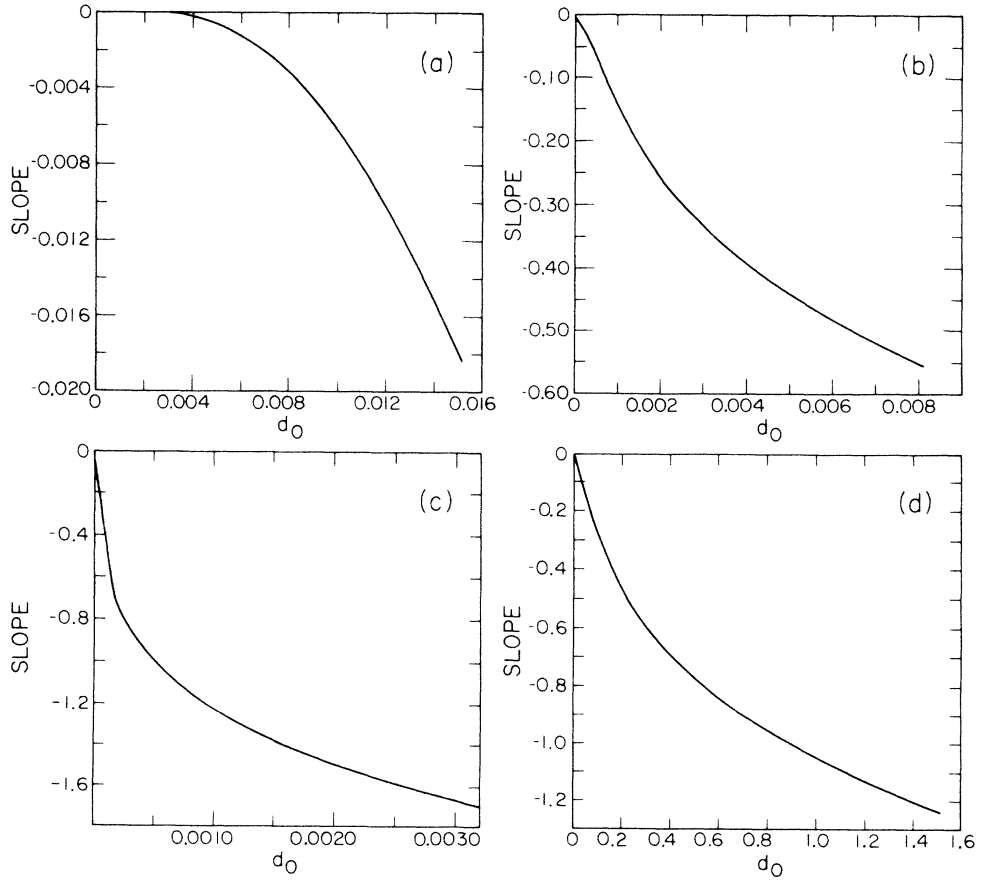

FIG. 1. A plot of the slope at the tip vs the capillarity parameter d_0 for (a) $\mathcal{N}_{\text{Péclet}}=1$; (b) $\mathcal{N}_{\text{Péclet}}=0.1$; (c) $\mathcal{N}_{\text{Péclet}}=0.01$; (d) $\mathcal{N}_{\text{Péclet}}=1$, $0<d_0<1.6$. Anisotropy parameter $\alpha=0$. Note that the slope is 0 only at $d_0=0$, corresponding to the Ivantsov solution.

sence of anisotropy ($\alpha=0$). At small values of d_0, we employed a stretching of the variable x so that more points are concentrated at the tip. The stretching is of the form

$$x_i=(\Delta x i)^2 S_{10}(i)+\frac{i}{N}x_{\max}S_{01}i\ , \tag{3.1}$$

where

$$S_{10}=\tfrac{1}{2}-\tfrac{1}{2}\tanh[\tfrac{1}{4}(i-N/3)]\ ,$$

$$S_{01}=\tfrac{1}{2}+\tfrac{1}{2}\tanh[\tfrac{1}{4}(i-N/3)]\ .$$

As $d_0\to 0$ the correction due to curvature occurs over increasingly smaller length scales and greater resolution at the tip is required in order to accurately calculate the slopes. The largest resolution attainable in this study with the available hardware (a Digital Equipment Corporation VAX 11/750 computer) was $N=100$ points, and this places a limit on the smallest value of d_0 for which accurate results have been obtained.

In Fig. 1 we plot the slope measured at the tip versus the surface tension parameter d_0 for $\mathcal{N}_{\text{Péclet}}=0.01, 0.1, 1$, for values of d_0 indicated in the figure caption. The curves all emanate from the origin corresponding to the fact that the Ivantsov solution ($d_0=0$) has a vanishing slope at the tip.

For $\mathcal{N}_{\text{Péclet}}=1$ oscillation of the slope through zero was observed for values of $d_0<0.002$. However, the magnitude (10^{-4}) of the slope in this region is of the same order as the numerical noise and the details of the oscillation could not be reproduced reliably as the resolution was changed. The oscillation is therefore attributable to numerical inaccuracy rather than the possible existence of a steady state.

Note that for $d_0\ll 1$, as shown in Fig. 1 for $\mathcal{N}_{\text{Péclet}}=1$ the slope behaves in an essentially singular fashion as d_0 approaches zero. In Fig. 2 we have plotted the logarithm of the absolute value of the slope versus d_0 for $\mathcal{N}_{\text{Péclet}}=1$ on a log-log plot. The results are consistent with an asymptotic behavior of the form

$$S\sim\exp[-c/(d_0)^{1/2}],\quad d_0\ll 1 \tag{3.2}$$

where S is the slope at the tip and c is a constant. This behavior is in line with the predictions of Caroli *et al.*,[14] who employed singular perturbation methods for Eq. (2.19) in the limit $\Delta\to 1$ ($\mathcal{N}_{\text{Péclet}}\to\infty$). A similar behavior of the slope has been derived by Kruskal and Segur and by Langer in the context of the boundary layer model.[15] The implication of (3.2) is that there are no steady states in the limit $d_0\to 0$ with $\alpha=0$. The numerical approximations become very reliable for moderate values of d_0 and the behavior of the slope in this regime implies that no steady states exist in the presence of isotropic surface energy over a range of undercoolings and surface energies d_0.

It is, of course, still possible that nontrivial steady states exist for values of the Péclet number and d_0 smaller than those considered here. Further work with increased resolution is necessary to resolve this issue.

We next consider the variation of the slope in the presence of anisotropy. In Fig. 3 we have again plotted the slope versus d_0 for the fourfold anisotropic surface energy

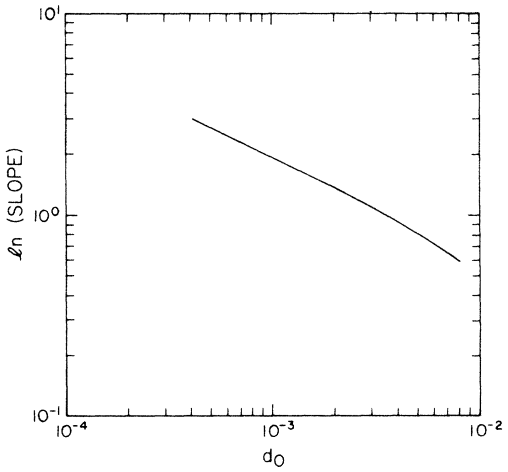

FIG. 2. A log-log plot of the logarithm of the slope for case (b) of Fig. 1. The approximate slope of the curve is -0.5 indicating that for small values of d_0 the slope decreases as $\exp[-c/(d_0)^{1/2}]$, where C is a constant.

given by (2.20). The results are shown for $\mathcal{N}_{\text{Péclet}}=1$, $\alpha=0.225$. In contrast to the isotropic case $\alpha=0$ the slope increases for small values of d_0 then decreases to cross zero at $d_0=0.0170$. This indicates the presence of a nontrivial steady needle crystal. The value of d_0 at which the slope vanishes was checked by running at different resolutions, and it was confirmed that the intersection point was insensitive to changes in the number of points used and the numerical parameters Δx and $x_{\max}$ [cf. (3.1)]. The resulting new steady state is shown in Fig. 4 along with the Ivantsov parabola corresponding to $\mathcal{N}_{\text{Péclet}}=1$. The anisotropic surface energy increases the curvature near the tip relative to the Ivantsov solution. In Fig. 5 we have plotted the relative difference between the anisotropy and the Ivantsov solution

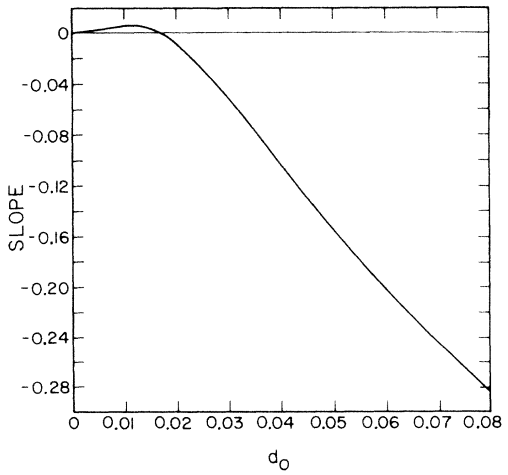

FIG. 3. A plot of the slope at the tip vs d_0 for $\mathcal{N}_{\text{Péclet}}=1$, $\alpha=0.227$. Note that the slope is 0 at $d_0=0$ (the Ivantsov solution) and at $d_0=0.0169$, indicating the existence of a nonisothermal steady state in the presence of anisotropic capillarity.

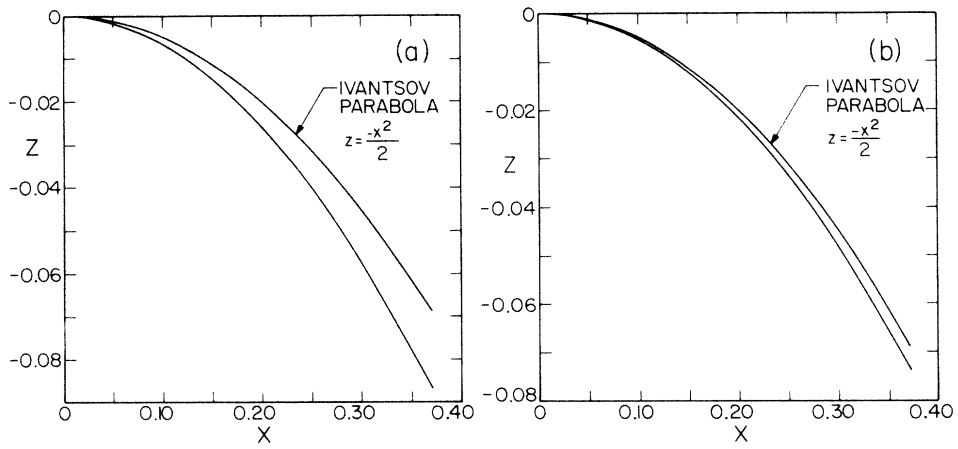

FIG. 4. A plot of the interface of the steady state corresponding to (a) $\mathcal{N}_{\text{Péclet}}=1$, $\alpha=0.2247$ and (b) $\mathcal{N}_{\text{Péclet}}=1$, $\alpha=0.0665$. The Ivantsov parabola $z=-x^2/2\mathcal{N}_{\text{Péclet}}$ is plotted for comparison. Note that the effect of the anisotropy is to enhance the curvature at the tip. Note also that as the anisotropy is lowered the steady state approaches the Ivantsov solution.

$$\left|\frac{z(x)-(-x^2/2\mathcal{N}_{\text{Péclet}})}{(-x^2/2\mathcal{N}_{\text{Péclet}})}\right| \tag{3.3}$$

as a function of x. The effect of the anisotropic surface energy is seen to be confined to a thin layer about the tip. This is also seen in Fig. 6, where we plot the temperature as a function of x for the case considered above. The temperature is lowered with respect to the Ivantsov value by the curvature near the tip and then rapidly recovers to the Ivantsov value as x increases. Once the steady solution is computed the representation (2.12) may be used to determine the temperature both inside and outside the solid. In Fig. 7 we have plotted the isotherms for $\mathcal{N}_{\text{Péclet}}=1$, $\alpha=0.225$. For comparison the Ivantsov solution, while possessing a heat boundary layer in the region exterior to the tip, is isothermal in the region interior to the solid-liquid interface.[16] The solution in the presence of anisotropy is not isothermal in the solid but the variation in temperature is small for $\mathcal{N}_{\text{Péclet}}=1$. In Fig. 7(b) we have plotted the isotherms for a small region near the tip of the needle. The numerical solution indicates that while the temperature drop recovers quickly to the Ivantsov value along the interface, recovery to the Ivantsov value in the core occurs at greater distances along the vertical.

We have also studied the variation of interface velocity and radius of curvature at the tip as a function of Péclet number. Our data covers the range $0.01<\mathcal{N}_{\text{Péclet}}<1$. As discussed in Sec. II, the value of d_0 at which nontrivial steady states occur is in fact a linear measure of the velocity since it is scaled by the diffusion length. For a given material

$$d_0=\frac{d_{0M}v}{2D}\ , \tag{3.4}$$

where $d_{0M}=\gamma/L$ is the intrinsic surface energy length of the material. Thus d_0 can also be interpreted as a dimensionless velocity. Similarly in our units the radius of curvature at the tip is also scaled by the diffusion length. The dimensionless radius of curvature ρ is equal to $-2C_1$ from (2.25) and is related to the unscaled radius of curvature ρ' by

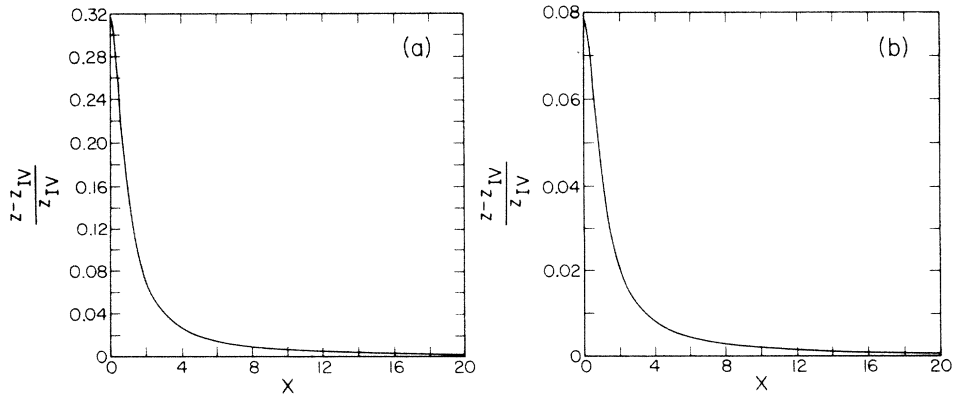

FIG. 5. A plot of the relative difference between the nonisothermal steady state and the Ivantsov needle $[z(x)-z_{\text{Ivantsov}}]/z_{\text{Ivantsov}}$ for (a) $\mathcal{N}_{\text{Péclet}}=1$, $\alpha=0.2247$ and (b) $\mathcal{N}_{\text{Péclet}}=1$, $\alpha=0.0665$.

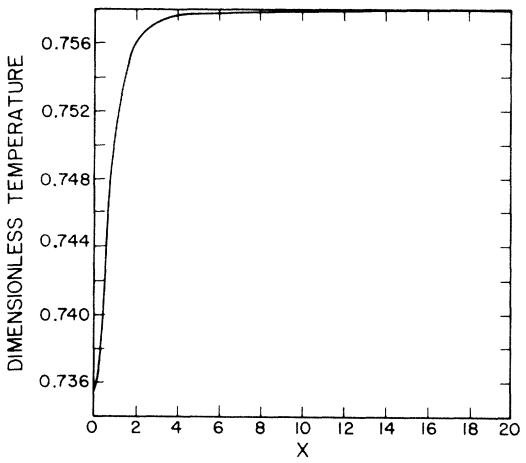

FIG. 6. A plot of the interfacial temperatures as a function of interface position x for $\mathcal{N}_{\text{Péclet}}=1$, $\alpha=0.2247$. The effect of the capillarity is to lower the temperature in a narrow region about the tip. At larger distances the temperature asymptotes to the Ivantsov value $\Delta=0.7578$.

$$\rho=\frac{v\rho'}{2D}\ .$$

Of physical and experimental interest is the behavior of the velocity and radius of curvature at small undercoolings. In Fig. 8 we have plotted the dimensionless velocity as a function of undercooling on a linear and logarithmic scale for various values of the anisotropy parameter α. As the undercooling decreases the velocity exhibits power-law behavior.[17] The value of the exponent is independent of the anisotropy as the curves become parallel in this region. Scaling behavior is also plainly evident in Fig. 9 where the dimensionless radius of curvature is plotted with respect to the velocity. The value of the slope for all values of α considered is very close to $\frac{1}{2}$, indicating that

$$\rho=F(\alpha)v^{1/2} \tag{3.5}$$

or

$$\rho'=G(\alpha)v^{-1/2}\ .$$

Thus, as the velocity increases the dendrite tip becomes sharper.

Pelcé and Pomeau have shown that (3.5) is essentially a consequence of the existence of a nontrivial steady state at low Péclet numbers. In our work we have taken as our unit of length the diffusion length l. This is a rather inconvenient scaling at low $\mathcal{N}_{\text{Péclet}}$ since l must diverge in this limit. Following Pelcé and Pomeau, if we scale all lengths with respect to the radius of curvature of the Ivantsov parabola ρ_I, then Eq. (2.22) becomes

$$\Delta+\frac{d_0}{\rho_I}\frac{\dfrac{d^2z}{dx^2}}{\left[1+\left[\dfrac{dz}{dx}\right]^2\right]^{3/2}}=\frac{1}{\pi}\mathcal{N}_{\text{Péclet}}\int_{-\infty}^{\infty}dx'\exp\{\mathcal{N}_{\text{Péclet}}[z(x')-z(x)]\}K_0(\mathcal{N}_{\text{Péclet}}\{(x'-x)^2+[z(x')-z(x)]^2\}^{1/2})\ . \tag{3.6}$$

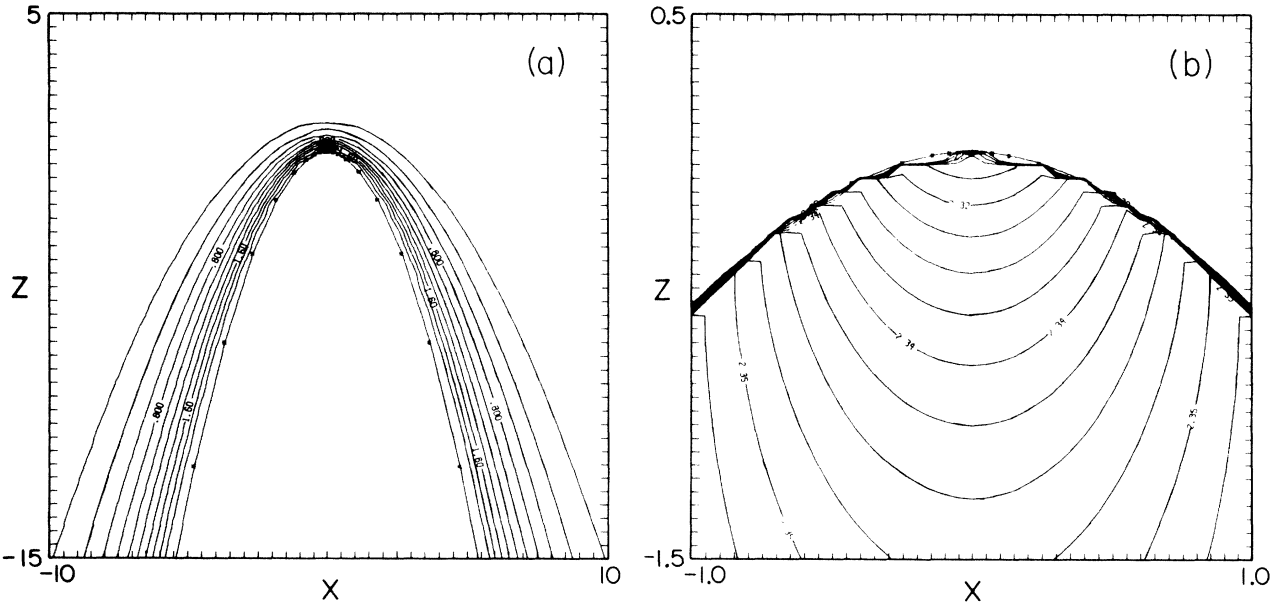

FIG. 7. A contour plot of the isotherms for the steady state corresponding to $\mathcal{N}_{\text{Péclet}}=1$, $\alpha=0.2247$. (a) The exterior of the interface. (b) A magnification of the region near the tip. The asterisks represent the collocation points used to compute the interface. The jaggedness of some of the contours in (b) is due to imperfections in the contouring algorithm.

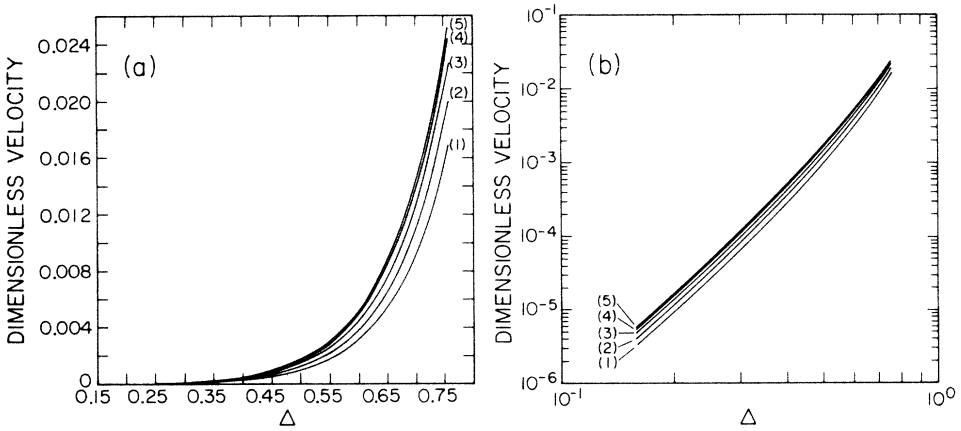

FIG. 8. A plot of the dimensionless velocity $d_{0M}v/2D$ vs undercooling for (1) $\alpha=0.227$, (2) $\alpha=0.3$, (3) $\alpha=0.4$, (4) $\alpha=0.5$, (5) $\alpha=0.6$ on (a) linear axes and (b) logarithmic axes. As $\Delta\rightarrow 0$, the behavior is consistent with $v\propto\Delta^4$.

Subtracting from both sides of the Ivantsov solution and evaluating the special functions in the limit $\mathcal{N}_{\text{Péclet}}\rightarrow 0$ yields the result

$$\frac{\dfrac{d^2z}{dx^2}}{\left[1+\left[\dfrac{dz}{dx}\right]^2\right]^{3/2}}=\frac{1}{\pi}\frac{\rho_I}{d_0}\mathcal{N}_{\text{Péclet}}\int_{-\infty}^{\infty}dx'\ln\left[\frac{(x'-x)^2+[z(x')-z(x)]^2}{(x'-x)^2+(x'^2-x^2)^2}\right]^{1/2}. \tag{3.7}$$

Thus in this limit, if a solution to Eq. (3.6) exists,

$$\rho_I^2 v=\text{const}\ , \tag{3.8}$$

and from the Ivantsov relation (2.18)

$$\Delta=\sqrt{\pi}(\mathcal{N}_{\text{Péclet}})^{1/2}\exp(\mathcal{N}_{\text{Péclet}})\operatorname{erfc}(\mathcal{N}_{\text{Péclet}})^{1/2}$$

it is seen that for $\mathcal{N}_{\text{Péclet}}\ll 1$,

$$v=E\Delta^4\ , \tag{3.9}$$

where the constant of proportionality E depends on the material properties but not on Δ. An examination of the slope in Fig. 8 shows that the tip radii calculated from (2.22) are consistent with (3.8).

In deriving (3.7) and (3.8) we have used the Ivantsov radius as a unit of length, but the scaling relations will apply equally well to the full nonlinear theory (2.22) at low $\mathcal{N}_{\text{Péclet}}$, provided that there is to first order a linear relationship between the true radius of curvature and ρ_I. That this is the case can be seen from Fig. 10, where the

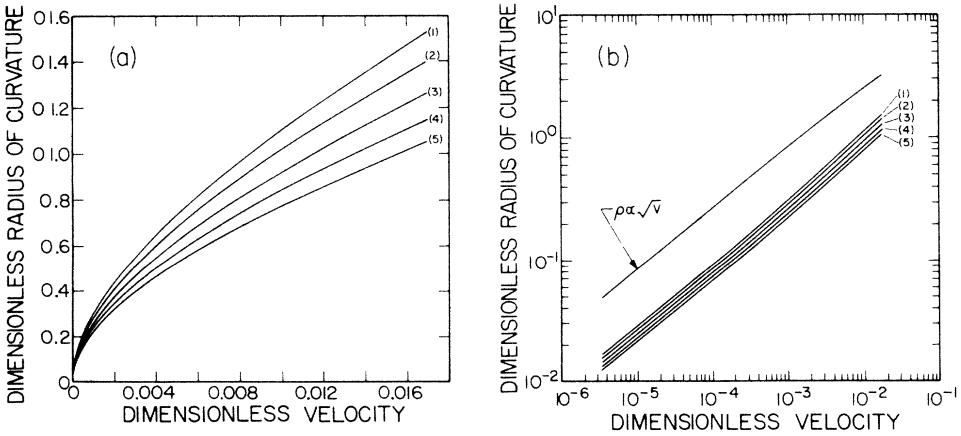

FIG. 10. A plot of the dimensionless radius of curvature $\rho' v/2D$ vs the dimensionless Ivantsov radius of curvature $\rho_I v/2D$ for values of the anisotropy parameter as given in the caption of Fig. 8. For comparison we have plotted the curve $\rho=\rho_I$.

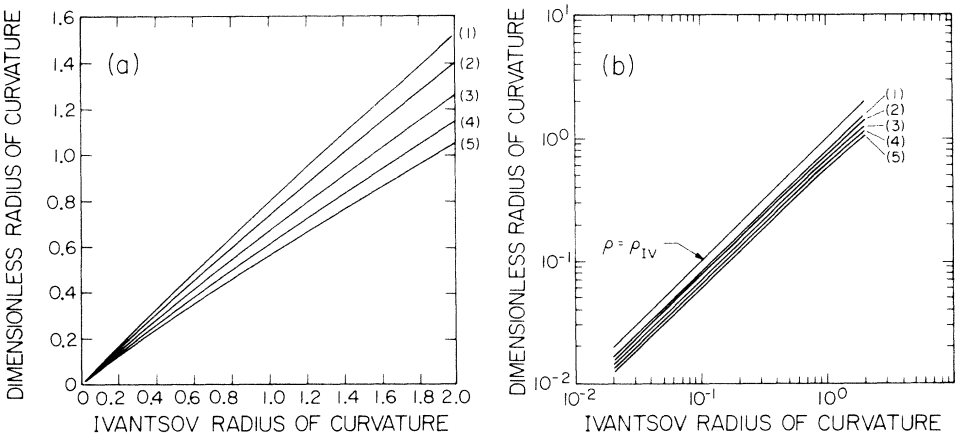

FIG. 10. A plot of the dimensionless radius of curvature $\rho' v/2D$ vs the dimensionless Ivantsov radius of curvature $\rho_I v/2D$ for values of the anisotropy parameter as given in the caption of Fig. 8. For comparison we have plotted the curve $\rho=\rho_I$.

dimensionless radius of curvature (effectively the tip Péclet number) is plotted relative to the dimensionless radius of curvature of the Ivantsov solution (which is just the Péclet number $\mathcal{N}_{\text{Péclet}}$).

IV. CONCLUSION

We have used boundary integral methods to derive a nonlinear integral equation for the shape of a needle crystal advancing steadily into an undercooled melt. The most important result of this study is a verification that the selection of steady states is a consequence of a nonlinear solvability criterion as discussed by Kessler *et al.*[18] and Ben Jacob *et al.*[8] This conclusion hinges on the assumption that these new states are stable. The examination of the stability of these states is currently in progress.

Our study suggests in addition that anisotropy is crucial to the existence of needled crystals. Numerical simulations of geometrical models of interface growth have emphasized the importance of anisotropy in stabilizing the tip of the advancing dendrite.[18] Numerical and analytical investigations of the boundary layer model further indicate that no steady solutions (needle crystals) are possible unless the surface energy is assumed to be anisotropic. The results of the boundary layer model are presumably only quantitatively valid for large Péclet numbers but the numerical results reported here imply that the boundary layer model may be qualitatively accurate even at moderately small values of $\mathcal{N}_{\text{Péclet}}$. We cannot, however, rule out the possibility of the existence of steady states with isotropic surface energy at still lower values of $\mathcal{N}_{\text{Péclet}}$ but this is unlikely. Kessler *et al.*[19] have recently performed an analysis of (2.22) in the limit $\mathcal{N}_{\text{Péclet}}\to 0$. Their conclusion is again that steady solutions do not exist in the presence of isotropic surface energy.

The formulation described here is easily generalizable to the case of axisymmetric needle crystals. It is also straightforward to derive an integral equation when the diffusion constants are unequal. The main modification of (2.22) is the addition of an appropriate distribution of heat dipoles. In this way it is possible to calculate needle crystals in realistic geometries and growth conditions and ultimately to make contact with the recent experiments of Glicksman,[20] which measure the anisotropic corrections to the surface energy.

ACKNOWLEDGMENTS

I would like to thank Jim Langer, Yves Pomeau, Nigel Goldenfeld, Gabi Kotliar, and Alain Karma for stimulating discussions and for making their results available prior to publication. I would also like to acknowledge the hospitality of the Institute for Theoretical Physics, University of California at Santa Barbara, where much of this work was done. This work was partially supported by the U.S. Department of Energy, Office of Basic Energy Sciences, under Contract No. DE-AT03-76ER72012.

[1]G. P. Ivantsov, Dok. Akad. Nauk. SSSR **58**, 567 (1974); see also G. Horvay and J. W. Cahn, Acta Metall. **9**, 695 (1961).

[2]M. E. Glicksman, R. J. Schaefer, and J. D. Ayers, Metall. Trans. A **7a**, 1747 (1976).

[3]J. S. Langer and H. Muller-Krumbhaar, Acta Metall. **26**, 1681 (1978).

[4]J. S. Langer, Rev. Mod. Phys. **52**, 1 (1980).

[5]G. C. Nash and M. E. Glicksman, Acta Metall. **22**, 1283 (1974).

[6]Previous implementations of the marginal stability hypothesis have used this assumption but it is not strictly necessary. A different interpretation can be found in E. Ben-Jacob, N. D. Goldenfeld, B. G. Kotliar, and J. S. Langer, Phys. Rev. Lett. **53**, 2110 (1984).

[7]R. C. Brower, D. A. Kessler, J. Koplik, and H. Levine, Phys. Rev. A **29**, 1335 (1984); Phys. Rev. Lett. **51**, 1111 (1983).

[8]E. Ben-Jacob, N. D. Goldenfeld, J. S. Langer, and G. Schon, Phys. Rev. Lett. **51**, 1930 (1983); Phys. Rev. **29**, 330 (1984).

[9]D. Kessler, J. Koplik, and H. Levine, Phys. Rev. A **31**, 1712 (1985); A. Karma and B. G. Kotliar, Phys. Rev. A **31**, 3266 (1985).
[10]J. S. Langer and L. A. Turski, Acta Metall. **25**, 1113 (1977).
[11]P. Pelcé and Y. Pomeau, Stud. Appl. Math. (to be published).
[12]J. W. McLean and P. G. Saffman, J. Fluid Mech. **102**, 455 (1981).
[13]J.-M. Vanden-Broeck, Phys. Fluids **26**, 2033 (1983).
[14]B. Caroli, C. Caroli, B. Roulet, and J. S. Langer, Phys. Rev. A **33**, 442 (1986).
[15]M. Kruskal and H. Segur (unpublished); J. S. Langer, Phys. Rev. A **33**, 435 (1986).
[16]H. Muller-Krumbhaar and J. S. Langer, Acta Metall. **26**, 1697 (1978).
[17]We have not included for comparison a curve of the form $v \propto \Delta^4$ in Fig. 8 because corrections due to finite Péclet number are substantial even at the value $\mathcal{N}_{\text{Péclet}}=0.01$ which is the smallest value considered here.
[18]D. A. Kessler, J. Koplik, and H. Levine (unpublished).
[19]D. A. Kessler and H. Levine (unpublished).
[20]S. C. Huang and M. E. Glicksman, Acta Metall. **29**, 701 (1981).